Proceedings of the ASME 2013 International Design Engineering Technical Conferences and
Computers and Information in Engineering Conference
IDETC/CIE 2013
August 4-7, 2013, Portland, Oregon, USA

DETC2013-12753

ORIGAMI ROTORS: IMPARTING CONTINUOUS ROTATION TO A MOVING PLATFORM USING COMPLIANT FLEXURE HINGES

Matthew S. Moses *

Independent Consultant
Lafayette, Colorado
Email: mmoses152@gmail.com

M. Kendal Ackerman †
Gregory S. Chirikjian ‡
Department of Mechanical Engineering
Johns Hopkins University
Baltimore, Maryland, 21218
Email: mkackerman@gmail.com, gregc@jhu.edu

ABSTRACT

A mechanism that admits continuous free rotation between a fixed platform and a rotating body is described. The mechanism is a serial kinematic chain with several revolute joints. The end of the kinematic chain has free and unlimited rotational motion, equivalent to a standard mechanical pivot, but the travel of each individual joint in the chain is limited to less than ±70 degrees. The joints that compose the chain can thus be constructed using compliant flexure hinges. The entire mechanism can be folded from a single flat sheet of material, and is thus well suited for self-assembly by folding, which is an increasingly attractive technique for building micro-scale devices. Potential applications include rotating propellers for micro underwater or fluid-immersed (e.g. within a blood vessel) robots, and high-mobility wheel-legs for crawling vehicles.

NOMENCLATURE

$s \in \mathbb{R}$ length along backbone curve
$t \in \mathbb{R}$ time coordinate
$\mathbf{r}(s,t) \in \mathbb{R}^3$ a point on backbone curve
$\mathbf{T},\mathbf{N},\mathbf{B} \in \mathbb{R}^3$ tangent, normal, and binormal vectors
$\mathbf{Q},\mathbf{R} \in \mathbb{R}^3$ vectors defining backbone ribbon
$p_1 \ldots p_4 \in \mathbb{R}$ backbone curve parameters
$C \in \mathbb{R}$ scale factor for backbone curve
$\phi \in \mathbb{R}$ angle to plane containing backbone curve
$\alpha \in \mathbb{R}$ angle of ribbon twist
$\omega_i \in \mathbb{R}^3$ direction of joint axis i
$q_i \in \mathbb{R}^3$ a point on joint axis i
$g_i \in SE(3)$ configuration of link i
$\xi_i \in \mathbb{R}^6$ twist for joint axis i
$\hat{\xi}_i \in se(3)$ twist for joint axis i
$\theta \in \mathbb{R}^{13}$ joint angles for half chain
$V_{13}^s \in \mathbb{R}^6$ spatial velocity of the rotor
$J(\theta) \in \mathbb{R}^{6\times 13}$ manipulator Jacobian for half chain
$A(\theta) \in \mathbb{R}^{13\times m}$ nullspace of $J(\theta)$
$m \in \mathbb{R}$ dimension of self-motion manifold tangent space
$k_r \in \mathbb{R}$ relaxation gain
$k_g \in \mathbb{R}$ backbone curve fitting gain
$d_i \in \mathbb{R}$ distance from link i to backbone curve
$P(\theta) \in \mathbb{R}$ sum of squared distances
$\bar{\theta} \in \mathbb{R}^{26}$ joint angles for full chain

1 INTRODUCTION

Many ingenious techniques are currently under development that use the principles of paper folding to create mechanical devices [1]. Folded mechanisms relying on flexure hinges have been demonstrated in such diverse areas as micro-flying vehicles [2, 3], legged vehicles [4, 5], self-assembling structures [6, 7, 8],

*Address all correspondence to this author.
†Graduate Research Assistant
‡Professor of Mechanical Engineering

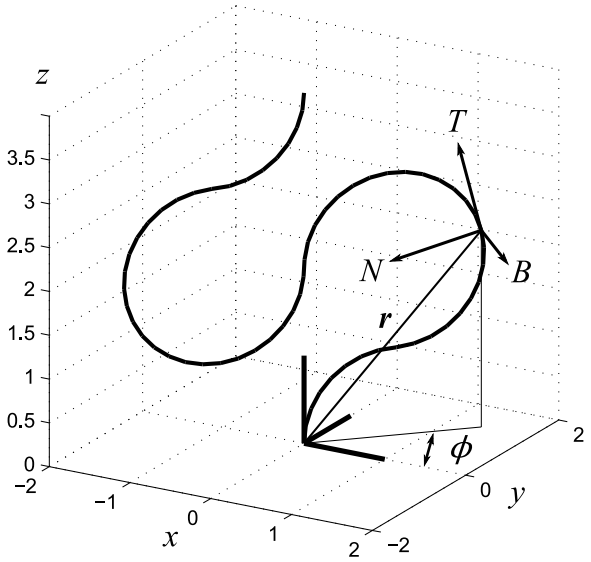

FIGURE 1. THE BACKBONE IS DEFINED AS A PLANAR PARAMETRIC CURVE $\mathbf{r}(s,t)$. THE ANGLE TO THE PLANE OF THE CURVE ϕ INCREASES LINEARLY WITH TIME t. THE STANDARD FRENET-SERRET FRAME COMPRISES THE VECTORS T, N, AND B.

and mesoscale grippers [9, 10] . Notwithstanding these remarkable devices, there seems to be a tacit assumption among the research community that it is impossible to build a device relying entirely on flexure hinges that provides continuous rotation to a spinning component. In this paper, we show how a technique commonly used in medical centrifuges can be used to create "origami rotors", or flexure-based mechanisms that impart unlimited rotation between a fixed base and a moving platform.

In 1971, a patent [11] was granted on a device that allows electrical power to be transmitted to a spinning platform without the need for a slip ring. Essentially, the electrical wires are held in a carriage that rotates (by means of gears) at half the speed of the spinning platform (which is supported by a shaft and bearings). This intriguing device was introduced to a popular audience in a *Scientific American* article [12], which included an illustration of how the principle could be demonstrated with a strip of paper. The technique does not seem to have gained much usage in electrical applications, but it is widely used to eliminate the need for rotating seals in medical centrifuges (e.g. [13, 14]).

The contributions of this paper include 1) explicit construction of a backbone curve and "guiding ribbon" which can be used as a template for generating continuous rotation motion in arbitrary kinematic chains; 2) specification of a chain of discrete kinematic subunits that is well suited for fitting the motion of the guiding ribbon; 3) determination of joint-space trajectories that generate continuous rotation in this chain; 4) a 2D layout for producing complete rotor mechanisms via folding.

TABLE 1. BACKBONE CURVE PARAMETERS

$s \in$	$[0, \frac{1}{8})$	$[\frac{1}{8}, \frac{1}{2})$	$[\frac{1}{2}, \frac{7}{8})$	$[\frac{7}{8}, 1]$
p_1	0	π	0	π
p_2	1	1	-1	-1
p_3	1	-1	-1	1
p_4	0	2	2	4

The reader may note similarities between the kinematics of our device and mechanisms such as a Turbula® or Inversina® tumbler mixer, a cowboy's spinning lariat, and the well-known Bricard linkage. Similarities to the first three of these items is purely superficial. In the Turbula and Inversina, the base of each mixer arm is continuously rotated by the drive system, ruling out the possibility of using flexure joints. And the cowboy, spinning his rope, must allow the free end to untwist so that it will not wind up and tangle [15]. The trihedral 6R Bricard linkage (also known as a Kaleidocycle, Flexahedron, or Schatz Invertible Cube) is a ring of six links connected by revolute joints [16]. Continuous *relative* rotation between separate links is possible with this mechanism, since the entire linkage can "fold in on itself" indefinitely. However, unlike our design, there is no means by which a stationary platform may make uninterrupted contact with any part of the mobile linkage.

One caveat to our design is that the chain which connects the fixed platform to the rotor must make a complete orbit around the rotor as it rotates. While this rules out the use of our mechanism as, for example, a wheel on an axle, there are many other possible applications in which it might be useful. Possibilities include: rotating a coil in a magnetic field, rotating propellers in a fluid, rotating a mass to serve as a gyroscopic sensor or momentum wheel, and rotating chain structures to serve as wheel-legs in crawling vehicles. While origami-like techniques have been used to create successful flying [3] and crawling [4] vehicles, in addition to gyroscopic sensors [17], there may be certain scenarios where an alternative mechanism using continuous rotation is advantageous. Further, our mechanism provides the entirely new ability to assemble, by folding, a device which continuously rotates a payload supported from a fixed base. This "new tool in the toolbox" for origami-based machine designers may have currently unanticipated applications.

2 BACKBONE CURVE AND GUIDING RIBBON

The problem of identifying a suitable pattern of motion for this mechanism is quite similar to the problem of determining gaits for snake-like robots, a topic that has received considerable interest. In a typical gait finding problem, the desired shape of

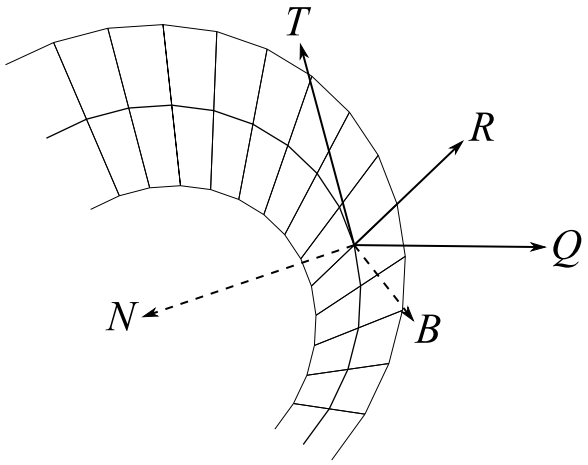

FIGURE 2. CLOSEUP OF BACKBONE AND RIBBON, SHOWING THE VECTORS DEFINING THE DESIRED LINK FRAME, Q, R, AND T. THE STANDARD FRENET-SERRET FRAME COMPRISES THE VECTORS T, N, AND B.

the snake at an instant in time is defined by a curve in $\mathbb{R}^3$, called the "backbone curve". The mechanical snake mechanism, usually made up of discrete segments, is then controlled so as to approximate the ideal shape of the backbone curve [18, 19]. However, in the present application, a curve in $\mathbb{R}^3$ by itself does not provide enough information to specify to the mechanism shape. The "roll" or twist of the coordinate frame relative to the naturally defined Frenet-Serret frame is also essential in correctly defining the mechanism trajectory.

Constructing the sequence of motion for the mechanism begins with defining a backbone curve. While curvature and torsion are sufficient to define any backbone curve [20], our chosen curve is easily defined by direct construction of its Frenet-Serret frame. A frame on the backbone is defined by a translation vector $\mathbf{r}(s,t)$ and three unit vectors $\mathbf{T}(s,t)$, $\mathbf{Q}(s,t)$, and $\mathbf{R}(s,t)$. The backbone curve itself is planar, but an additional roll component is applied to determine the "twist" of a ribbon, which is overlaid on the backbone.

Figure 1 shows the backbone curve. The quantity s is a parameter that varies from 0 to 1 along the length of the curve. The shape of the curve varies with time, which is parameterized with t. The curve is constructed piecewise from four circular arc segments by

$$\alpha(s,t) = \phi(t) + p_1, \tag{1}$$

$$\mathbf{r}(s,t) = C \begin{bmatrix} p_2 \cos\big(\phi(t)\big)\big(1-\cos(4\pi s)\big) \\ p_2 \sin\big(\phi(t)\big)\big(1-\cos(4\pi s)\big) \\ p_3 \sin(4\pi s) + p_4 \end{bmatrix}, \tag{2}$$

$$\mathbf{T}(s,t) = \begin{bmatrix} p_2 \cos\big(\phi(t)\big)\sin(4\pi s) \\ p_2 \sin\big(\phi(t)\big)\sin(4\pi s) \\ p_3 \cos(4\pi s) \end{bmatrix}, \tag{3}$$

$$\mathbf{N}(s,t) = \begin{bmatrix} p_2 \cos\big(\phi(t)\big)\cos(4\pi s) \\ p_2 \sin\big(\phi(t)\big)\cos(4\pi s) \\ -p_3 \sin(4\pi s) \end{bmatrix}, \tag{4}$$

where the six parameters p_1 to p_6 depend on which of the four segments the point of interest lies in. These parameters are given in Table 1. The scalar C simply controls the overall size of the backbone curve. The time varying angle $\phi(t)$ can be an arbitrary function, however a natural choice is $\phi(t) = 2\pi t$, so the backbone will make one complete cycle as t varies from 0 to 1.

For each point along the backbone, the binormal vector $\mathbf{B}$ is given by

$$\mathbf{B} = \mathbf{T} \times \mathbf{N} = p_2 p_3 \begin{bmatrix} -\sin\big(\phi(t)\big) \\ \cos\big(\phi(t)\big) \\ 0 \end{bmatrix}.$$

The twist of the ribbon is defined by creating a new frame $\{\mathbf{Q},\mathbf{R},\mathbf{T}\}$ that results from rotating the vectors $\mathbf{N}$ and $\mathbf{B}$ about $\mathbf{T}$ by the angle α

$$\begin{aligned} \mathbf{R}(s,t) &= \cos(\alpha)\mathbf{B} + \sin(\alpha)\mathbf{N} \\ \mathbf{Q}(s,t) &= \cos(\alpha)\mathbf{N} - \sin(\alpha)\mathbf{B}, \end{aligned}$$

as shown in Figure 2. Note that when $s = 1/2$ the desired frame is

$$\{\mathbf{Q},\mathbf{R},\mathbf{T}\}(1/2,t) = \begin{bmatrix} -\cos\big(2\phi(t)\big) & -\sin\big(2\phi(t)\big) & 0 \\ -\sin\big(2\phi(t)\big) & \cos\big(2\phi(t)\big) & 0 \\ 0 & 0 & -1 \end{bmatrix} \tag{5}$$

and the displacement vector from the origin to the frame is $\mathbf{r}(1/2,t) = (0,0,2C)^T$. Thus the frame at $s = 1/2$ spins in place about the z axis at a speed twice that of $\phi(t)$. Snapshots of the full ribbon as it rotates, as well as a link to an animation, are shown in Figure 3.

As an aside, while the animation in Figure 3 makes clear that our particular ribbon geometry makes a full rotation cycle without twisting, Călugăreanu's Theorem [21] provides conditions for "non twisting" motions of ribbons in general. A topic for future work is to investigate the implications of this theorem for devices like the one presented in this article.

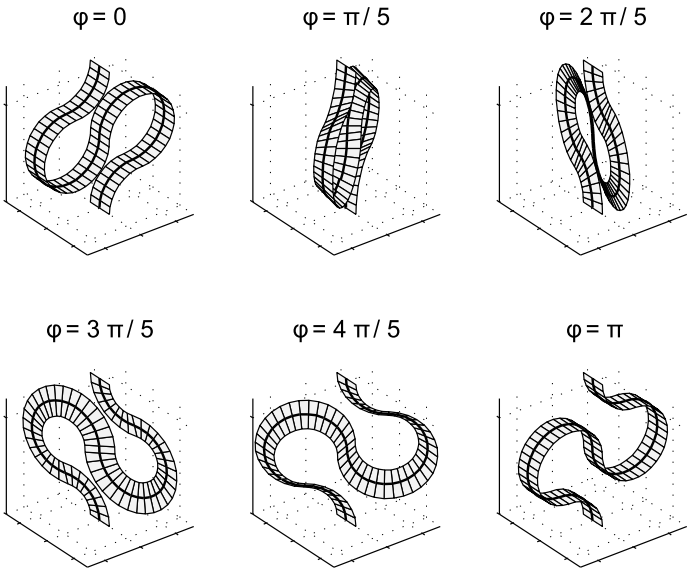

FIGURE 3. SNAPSHOTS OF THE RIBBON. AN ANIMATION OF THE RIBBON AS IT ROTATES IS AVAILABLE AT `http://youtu.be/ccKN-PoKFPo`

3 CHAIN KINEMATICS

We desire to make some form of mechanism that can support a rotating platform (the rotor) against its own weight, inertia and other disturbance forces. While it is possible to construct a flexible ribbon that moves in the manner of Figure 3, and place the rotor at its center, it is not clear how the deformation could be actuated in a controlled manner. This section describes a snake-like serial kinematic chain, made of a sequence of linked tetrahedra, that closely approximates the motion of the ribbon while being easy to construct and control. Kinematically similar snake-like mechanisms are well known, and can be easily constructed from folded strips of paper (e.g. [22]).

We begin by describing a "half chain" that mimics the motion of the ribbon from the base up to the rotor. The other half of the chain is easily constructed by symmetry. There are 13 joints in the half chain. Joint i connects rigid links i and $i-1$. The base link (link 0) is fixed. The chain is made up of three types of links, as shown in Figure 4. The two types of tetrahedra (identical except for attachment of their coordinate frames) alternate along the chain. This alternating arrangement of links is reminiscent of the construction of the Bricard linkage, and is also identical to that used in many snake-like robots. The number and arrangement of the links are chosen out of convenience, and this particular chain is not claimed to be optimal.

Using the product of exponentials formulation [23], the configuration of the ith link is obtained by

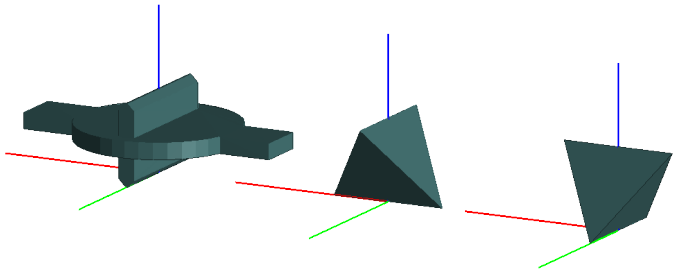

FIGURE 4. THE SNAKE-LIKE CHAIN IS MADE UP OF THREE TYPES OF LINKS: TWO ALTERNATING TETRAHEDRA AND THE ROTOR.

$$g_i(\theta) = \left(\prod_{k=1}^{i} \exp\left(\widehat{\xi}_k \theta_k\right) \right) g_{i_0}. \tag{6}$$

The initial configuration of each link is given by the 4×4 matrix

$$g_{i_0} = \begin{bmatrix} I_{3\times 3} & q_i \\ 0_{1\times 3} & 1 \end{bmatrix}, \tag{7}$$

where q_i is a point on the ith joint axis, $q_i = (0,0,(i-1))^T$. The axis of rotation of each joint is in the direction of $\omega_i = (0,1,0)^T$ for odd i, and $\omega_i = (1,0,0)^T$ for even i. The joint twists $\xi_i \in \mathbb{R}^6$ are given by

$$\xi_i = \begin{pmatrix} -\omega_i \times q_i \\ \omega_i \end{pmatrix}. \tag{8}$$

The joint twists $\widehat{\xi}_i \in se(3)$ are described in the Appendix.

The rotor is link 13, the last link of the half chain. The remaining portion of the chain, links 14 through 26, are arranged symmetrically to the first half, with the plane of symmetry intersecting the center of the rotor (see Figure 7). The kinematics of links 14 through 26 are identical to that of the first half of the chain, except $\omega_i = (0,1,0)^T$ for *even* i, and $\omega_i = (1,0,0)^T$ for *odd* i.

The "manipulator Jacobian" $J(\theta)$ relates joint velocities $\dot{\theta}$ to the spatial velocity of the rotor,

$$V_{13}^s = \left((\dot{g}_{13})\, g_{13}^{-1} \right)^{\vee} = J(\theta)\dot{\theta}. \tag{9}$$

$J(\theta)$ is a 6×13 matrix with a special structure that can be constructed iteratively, as described in the Appendix and in greater detail in [23]. The Jacobian plays a central role in finding suitable joint trajectories.

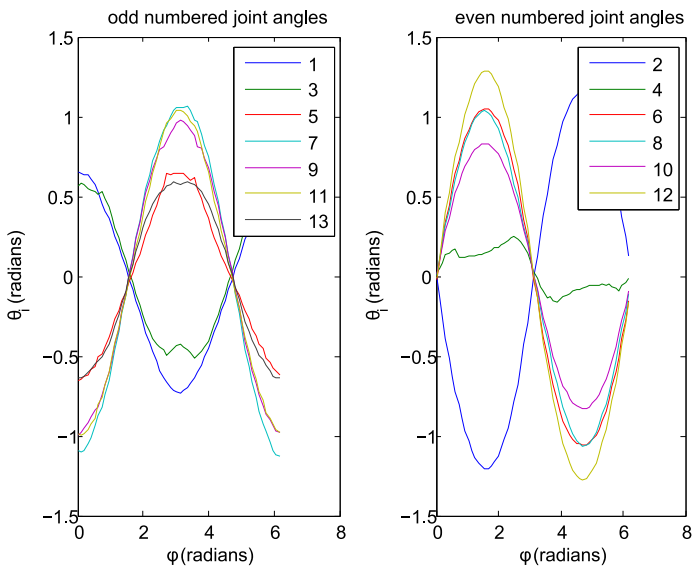

FIGURE 5. JOINT TRAJECTORY FOUND WITH THE "AUTOMATIC" METHOD. NUMBERS IN LEGEND INDICATE JOINT NUMBER. AN ANIMATION OF THE HALF CHAIN MOVING WITH THIS TRAJECTORY IS AVAILABLE AT `http://youtu.be/AGZfrXsbrTg`

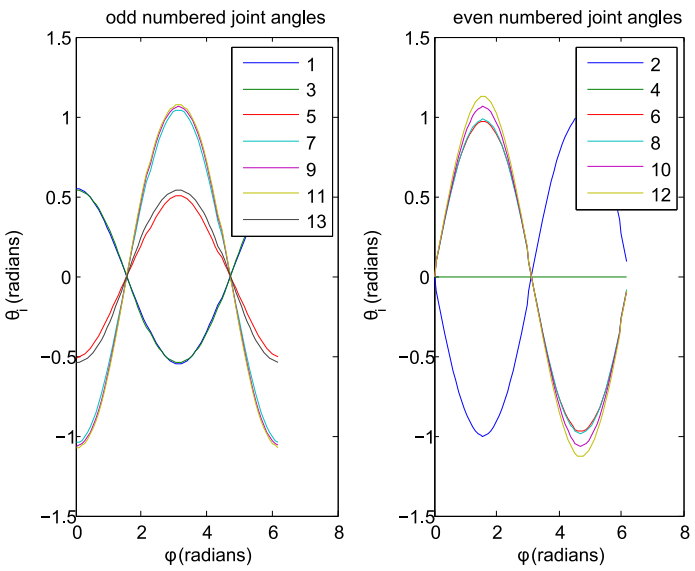

FIGURE 6. JOINT TRAJECTORY FOUND WITH THE "OPTIMIZED SINUSOID" METHOD. NUMBERS IN LEGEND INDICATE JOINT NUMBER. AN ANIMATION OF THE HALF CHAIN MOVING WITH THIS TRAJECTORY IS AVAILABLE AT `http://youtu.be/dp4zxvpw5og`

4 TRAJECTORY GENERATION

Given the kinematics of the chain, the next step is to identify time varying joint angles $\theta(t)$ that result in the motion of the chain closely approximating that of the ribbon. The initial joint space trajectory is found with a three step algorithm we call the "automatic" method. Then, this trajectory is further optimized using what we call the "optimized sinusoid" method.

To begin with, a set of evenly spaced angles ϕ_i are chosen in the interval $[0, 2\pi)$. Then, for each value of ϕ_i, the procedure is to 1) move the rotor to the desired frame, 2) relax the chain by application of torsion spring forces at each joint, 3) move the chain onto the ribbon by application of spring-like forces between the origin of each link and the backbone curve.

4.1 Trajectory - Step 1

First, for a given ϕ, the desired frame of the center of the rotor is given by Eq 5. A θ that places the rotor close to this desired configuration is computed using the well known inverse Jacobian method [23], where the desired velocity in joint space

$$\dot{\theta} = J^T (JJ^T)^{-1} V_{13}^s$$

is integrated numerically from an initial estimate (often $\theta = 0$), until the actual rotor configuration is within a close tolerance to the desired. In this case the pseudoinverse of the Jacobian is used because the kinematic chain is redundant. The desired spatial velocity at each step is given by

$$V_{13}^s = \left(\log(g_{des} g_{13}^{-1})\right)^\vee$$

where g_{des} is the desired configuration of the rotor, which is computed easily from Eq 5

$$g_{des} = \begin{bmatrix} -\cos(2\phi) & -\sin(2\phi) & 0 & 0 \\ -\sin(2\phi) & \cos(2\phi) & 0 & 0 \\ 0 & 0 & -1 & 2C \\ 0 & 0 & 0 & 1 \end{bmatrix}.$$

Some manual tuning of the scale factor C is required so that the length of the ribbon matches that of the chain, although the method is not especially sensitive to small variations in C. For the chain shown in Figure 7 a value of $C = 1.838$ was used.

4.2 Trajectory - Step 2

During the relaxation step, the desired joint velocity is given by

$$\dot{\theta}_{desired} = -k_r \theta,$$

where k_r is a scalar multiplier representative of the spring constant at each joint. With the rotor held fixed, the desired joint

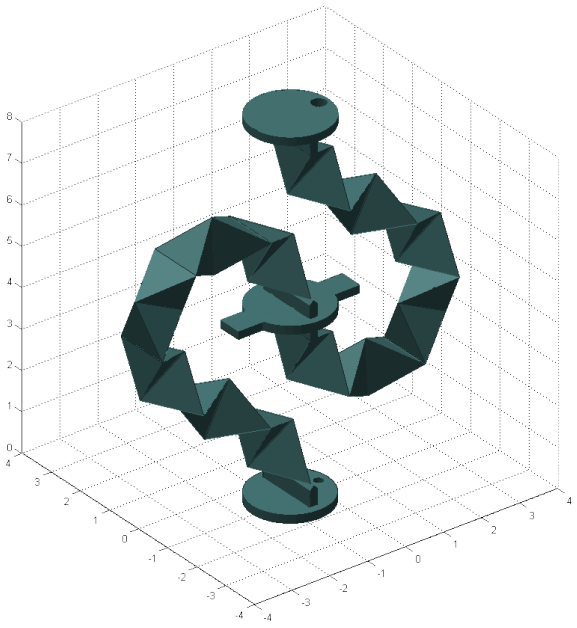

FIGURE 7. THE FULL SNAKE-LIKE CHAIN HAS 26 JOINTS, 24 TETRAHEDRA, 2 FIXED END PIECES, AND 1 ROTOR. AN ANIMATION OF THIS MECHANISM UNDERGOING CONTINUOUS ROTATION, USING THE SMOOTH TRAJECTORY IN FIGURE 6, IS AVAILABLE AT `http://youtu.be/gzq5gbF-QC8`

velocity $\dot{\theta}_{desired}$ is projected onto the tangent space of the self-motion manifold [23] at θ, resulting in the actual joint velocity to be integrated,

$$\dot{\theta} = A(\theta)A(\theta)^T \ \dot{\theta}_{desired}, \tag{10}$$

where $A(\theta)$ is the $13 \times m$ nullspace of $J(\theta)$, and m is the dimension of the self-motion manifold tangent space at θ. Each column of A represents a "direction" in which the chain can move without moving the rotor. For each value of ϕ, Eq 10 is integrated numerically for a certain amount of time. The main purpose of this step is to keep the chain from tangling on itself, and so the results are not especially sensitive to the integration time.

4.3 Trajectory - Step 3

The third step is to move the chain, as close as possible, onto the ribbon corresponding to the given ϕ. This is done in the same way as the relaxation step, except a different method is used to generate $\dot{\theta}_{desired}$,

$$\dot{\theta}_{desired} = -k_g \frac{\partial P}{\partial \theta}, \tag{11}$$

where P is a potential-like function given by

$$P(\theta) = \sum_{i=1}^{12} d_i^2,$$

and d_i is the minimum Euclidean distance from the origin of link i to the backbone curve. If necessary, additional terms can be added to P that account for rotational error, or distance from the link to a preferred segment of the backbone curve, but the simple version above gives satisfactory performance. Eq 11 is numerically integrated until the change in θ between time steps falls below an arbitrary threshold.

4.4 Trajectory - Output

The trajectory generated by this three step process is shown in Figure 5. It is interesting to see that this "automatic" method finds trajectories close to sinusoidal curves. This suggests that a careful choice of kinematics and joint trajectory could result in the desired motion using only simple sinusoids. Guided by the trajectory of Figure 5, we make an informed guess as to what a "pure sinusoid" trajectory might look like. Two sinusoidal signals, out of phase by 90 degrees, are used to generate the trajectories

$$\begin{aligned} f_A(t) &= (\pi/3)\cos(\phi(t)) \\ f_B(t) &= (\pi/3)\sin(\phi(t)). \end{aligned} \tag{12}$$

The trajectory of each joint angle is proportional to either f_A or f_B,

$$\begin{aligned} \theta_1 &= f_A/2 \\ \theta_2 &= -f_B \\ \theta_3 &= f_A/2 \\ \theta_4 &= 0 \\ \theta_5 &= -f_A/2 \\ \theta_6 &= f_B \\ \theta_7 &= -f_A \\ \theta_8 &= f_B \\ \theta_9 &= -f_A \\ \theta_{10} &= f_B \\ \theta_{11} &= -f_A \\ \theta_{12} &= f_B \\ \theta_{13} &= -f_A/2. \end{aligned} \tag{13}$$

This trajectory results in a motion that is fairly close to the desired, except that the rotor undergoes some slight wobbling as

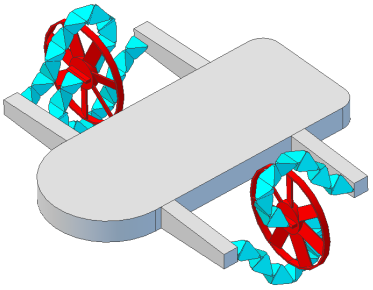

FIGURE 8. CONCEPTUAL DESIGN OF A SELF-ASSEMBLED ORIGAMI-BASED MICRO UNDERWATER (OR FLUID-IMMERSED) VEHICLE USING TWO PROPELLERS.

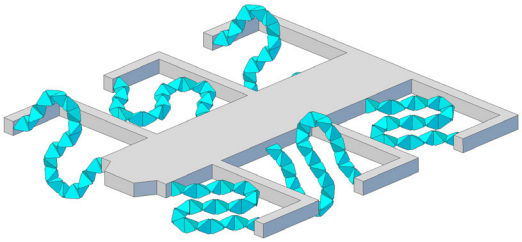

FIGURE 9. CONCEPTUAL DESIGN OF A SELF-ASSEMBLED, ORIGAMI-BASED CRAWLING VEHICLE. SIX ROTATING CHAINS SERVE AS WHEEL-LEGS IN AN ALTERNATING TRIPOD GAIT, IN THE MANNER OF RHex [24].

the system rotates. This slight wobble turns out to be easily corrected by using what we call the "optimized sinusoidal" method. The sinusoid trajectory above serves as the initial condition to the solver of Step 1 (Section 4.1). Only a small correction is necessary, and no further relaxation or backbone fitting steps are necessary. The output of this process is shown in Figure 6.

Once a suitable trajectory $\theta(t)$ has been found for the half chain (links 1 through 13), a trajectory $\bar{\theta}(t)$ for a full chain with 26 links is easily constructed using symmetry. The first thirteen joints of the full- and half- versions are of course identical, $\bar{\theta}_i = \theta_i$ for $i = 1...13$. The joint angles for the remainder of the full chain are given simply by

$$\begin{aligned} \bar{\theta}_{14} &= -\theta_{13} \\ \bar{\theta}_{15} &= -\theta_{12} \\ \bar{\theta}_{16} &= -\theta_{11} \\ &\cdots \\ \bar{\theta}_{26} &= -\theta_{1}. \end{aligned} \tag{14}$$

An image of the full chain, as well as a link to an animation of it in operation, are given in Figure 7.

5 APPLICATIONS AND IMPLEMENTATION

Two possible applications for the mechanism are shown in Figures 8 and 9. In the first, two rotor mechanisms are used to drive propellers in a micro underwater or fluid-immersed (e.g. within a blood vessel) vehicle. In the second, six rotor mechanisms serve as legs in a small hexapod crawling robot. In this case, the chains themselves provide the locomotive force as they rotate around. Flying platforms and legged vehicles made by origami techniques have already been successfully demonstrated [3, 4]. In most applications, it is admittedly unlikely that vehicles based on our mechanism would outperform existing designs. However, there are a few aspects in which our design may provide advantages. First, the rotating chain, rotating platform, and fixed platform can be produced from a single connected cutout pattern, as shown in Figure 11. The structural "fixed" joints are distinct from the moving "flexural" joints, thus making this design amenable to self-assembly by self-folding joints. Self-folding methods such as [8] might be easily adapted to produce micro-scale versions of the mechanism of Figure 11. A second potential advantage is that the higher density of actuators, and the fact that the rotor spins at twice the actuator frequency, may allow for higher specific power (i.e. greater mechanical power output for a given mechanism size) than comparable devices in the same size range.

In principle, it is possible to interface multiple rotating platforms together, as proposed in Figure 10. Each rotor has extended "paddles" that serve as crude gear teeth. The teeth mesh with each other as the rotors spin. This would require a complex trajectory that allows the chains to interleave within the paddles, so as to avoid collisions during rotation, since the chain must rotate (on average) at half the gear speed. We acknowledge that, beyond the amusement of folding entire assemblies of meshing gears from a single sheet of paper, it is not immediately clear what the application of this would be.

The sinusoid trajectory allows the entire mechanism to be driven by two sinusoidal drive signals, spaced 90 degrees out of phase. For example, suppose that each of the 26 flexure joints in the mechanism (Figure 7) were driven by a piezoelectric bending actuator, and further assume these actuators could achieve the full required ± 60 degrees of travel, then each bending actuator could be wired directly to one or the other of the drive sources. The driving electrical waveforms could be transmitted through the entire device using no more than four conductive traces. The motion of the entire mechanism could be controlled via a two-phase sinusoidal signal, with the relative phase of the signals, either leading or lagging by 90 degrees, controlling the direction of rotation. A wiring layout suitable for producing this pattern of motion in the actuators is shown schematically on the pattern in Figure 11. Also shown on the diagram are the polarity of the hypothetical "push-pull" actuators at each joint, where necessary, attenuating resistors to reduce the amplitude of the input

waveforms. The wiring layout is consistent with the trajectory definitions in Eq (13).

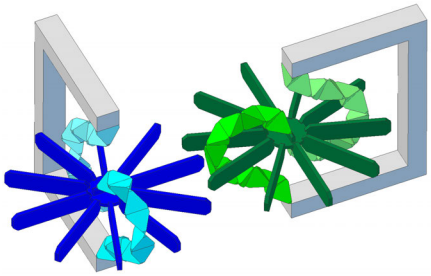

FIGURE 10. MESHING GEAR-LIKE MECHANISMS ARE THEORETICALLY POSSIBLE. A COMPLICATED TRAJECTORY IS REQUIRED TO ALLOW THE ROTATING CHAIN TO INTERLEAVE THE GEAR "TEETH" WHILE THE CHAIN ROTATES AT (ON AVERAGE) ONE HALF THE GEAR SPEED.

6 CONCLUSIONS AND FUTURE WORKS

This work illustrates an "existence proof" of a mechanism made with compliant flexure joints that can impart continuous rotation to a rotating platform, from a fixed base. Combined with other recent advances in folding- or origami-based robotics, this work may contribute toward applications such as self-assembling, micro-scale motors, gears, gyroscopes, turbines, pumps, and propellers.

Both a general ribbon model and a specific kinematic chain trajectory were presented. The ribbon model is useful because it can be used as a guiding shape for any arbitrary kinematic chain. The specific kinematic chain presented was chosen because it is a simple mechanism that can be constructed from a folded strip of paper, (e.g. [22]), and in principle actuated with piezoelectric (or other) bending actuators. A detailed joint trajectory for this device was constructed, and further reduced to a set of simple sinusoid curves. A possible means was proposed for producing the mechanism from a single sheet of material, incorporating embedding wiring and actuators, and potentially allowing the entire mechanism to self-assembly by folding.

Topics for future work include performing dynamic simulations to investigate torque and power requirements of the joint actuators, building a functional prototype, further exploring the design space for similar mechanisms, and exploring potential applications. Dynamic analysis may reveal that many of the joints that are currently actuated could simply be replaced by passive spring-loaded joints. It is likely that a more careful choice of kinematics may result in a mechanism that has fewer joints, is easier to control, and requires smaller joint excursions.

REFERENCES

[1] Greenberg, H., Gong, M., Magleby, S., and Howell, L., 2011. "Identifying links between origami and compliant mechanisms". *Mechanical Sciences,* ***2***, pp. 217–225.

[2] Avadhanula, S., and Fearing, R. S., 2005. "Flexure design rules for carbon fiber microrobotic mechanisms". In Robotics and Automation (ICRA), 2005 IEEE International Conference on.

[3] Wood, R., 2007. "Design, fabrication, and analysis of a 3DOF, 3cm flapping-wing MAV". In Intelligent Robots and Systems, 2007. IROS 2007. IEEE/RSJ International Conference on.

[4] Birkmeyer, P., Petersen, K., and Fearing, R., 2009. "DASH: A dynamic 16g hexapedal robot". In Intelligent Robots and Systems, 2009. IROS 2009. IEEE/RSJ International Conference on.

[5] Vogtmann, D., Gupta, S., and Bergbreiter, S., 2011. "Multi-material compliant mechanisms for mobile millirobots". In Robotics and Automation (ICRA), 2011 IEEE International Conference on.

[6] Nagpal, R., 2001. "Programmable self-assembly: Constructing global shape using biologically-inspired local interactions and origami mathematics". PhD thesis, Massachusetts Institute of Technology.

[7] Hawkes, E., An, B., Benbernou, N., Tanaka, H., Kim, S., Demaine, E., Rus, D., and Wood, R., 2010. "Programmable matter by folding". *Proceedings of the National Academy of Sciences of the United States of America,* ***107***, pp. 12441–12445.

[8] Bassik, N., Stern, G. M., and Gracias, D. H., 2009. "Microassembly based on hands free origami with bidirectional curvature". *Applied Physics Letters,* ***95(9)***.

[9] Hayes, G., Frecker, M., and Adair, J., 2011. "Fabrication of compliant mechanisms on the mesoscale". *Mechanical Sciences,* ***2***, pp. 129–137.

[10] Randhawa, J. S., Leong, T. G., Bassik, N., Benson, B. R., Jochmans, M. T., and Gracias, D. H., 2008. "Pick-and-place using chemically actuated microgrippers". *Journal of the American Chemical Society,* ***130***(51), pp. 17238–17239.

[11] Adams, D. A., 1971. Apparatus for providing energy communication between a moving and a stationary terminal.

[12] Stong, C. L., 1975. "The amateur scientist: Diverse topics, starting with how to supply electric power to something that is turning". *Scientific American*, Dec.

[13] Lolachi, H., 1978. Centrifugal liquid processing apparatus.

[14] Brown, R. I., 1978. Centrifugal apparatus with oppositely positioned rotational support means.

[15] Byers, C., 1966. *Cowboy Roping and Rope Tricks*. Dover Publications.

[16] Baker, J. E., 1980. "An analysis of the Bricard linkages". *Mechanism and Machine Theory,* ***15***, pp. 267–286.

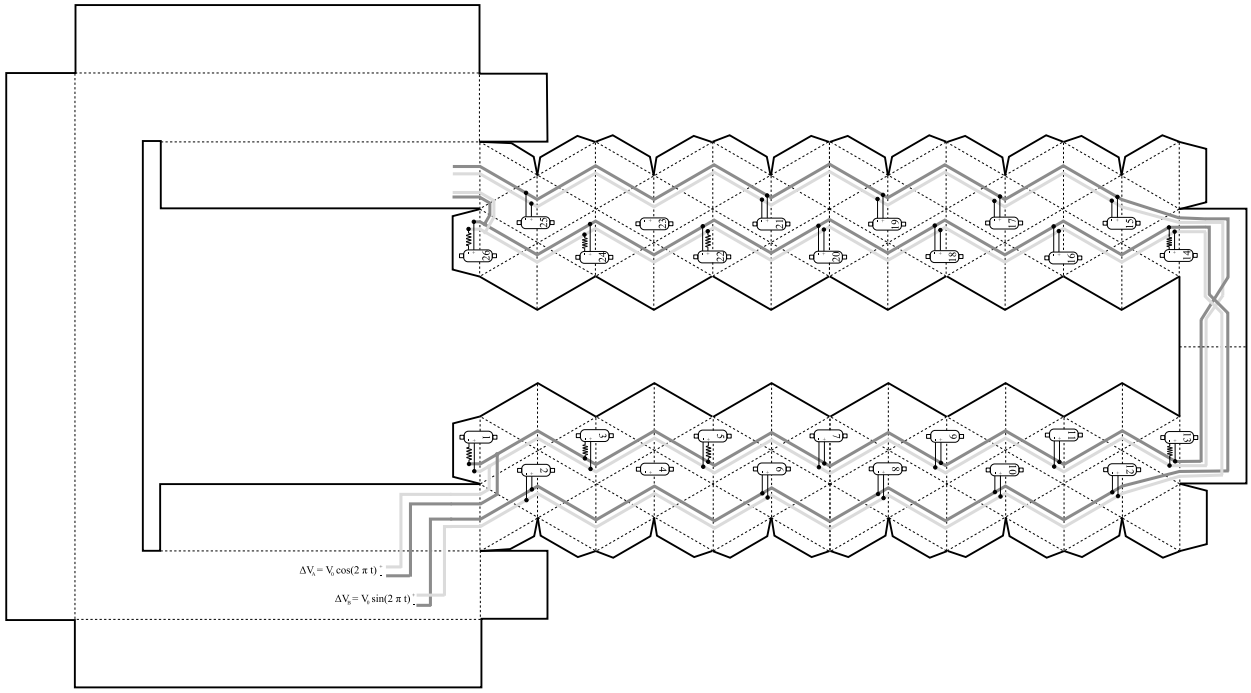

FIGURE 11. FOLDING TEMPLATE FOR BUILDING A FULL CHAIN MECHANISM. THIS PATTERN CAN BE ENLARGED AND CUT OUT TO BUILD A MODEL OF THE DEVICE. LOCATIONS FOR VOLTAGE-DRIVEN BENDING ACTUATORS ARE SHOWN, IN ADDITION TO WIRING LAYOUT, ACTUATOR POLARITY, ATTENUATING RESISTORS, AND SIGNAL SOURCES NECESSARY FOR PRODUCING CONTINUOUS ROTATION. THIS WIRING LAYOUT IMPLEMENTS THE TRAJECTORY DEFINED IN EQS (13) AND (14).

[17] Wu, W., Wood, R., and Fearing, R., 2002. "Halteres for the micromechanical flying insect". In IEEE International Conference on Robotics and Automation, ICRA 2002.

[18] Burdick, J. W., Radford, J., and Chirikjian, G. S., 1995. "A 'sidewinding' locomotion gait for hyper-redundant robots". *Advanced Robotics,* ***9***, pp. 195–216.

[19] Hatton, R. L., and Choset, H., 2009. "Generating gaits for snake robots by annealed chain fitting and keyframe wave extraction". In IEEE/RSJ International Conference on Intelligent Robots and Systems, pp. 840–845.

[20] Chirikjian, G. S., and Burdick, J. W., 1994. "A Modal Approach to Hyper-Redundant Manipulator Kinematics". *IEEE Transacations on Robotics and Automation,* ***10***(3), pp. 343–354.

[21] Dennis, M., and Hannay, J., 2005. "Geometry of Călugăreanu's Theorem". *Proceedings: Mathematical, Physical and Engineering Sciences,* ***461***, pp. 3245–3254.

[22] Schaedel, 2001. Folding puzzle/transformational toy with 24 linked tetrahedral elements.

[23] Murray, R. M., Li, Z., and Sastry, S. S., 1994. *A Mathematical Introduction to Robotic Manipulation*. CRC Press.

[24] Saranli, U., Buehler, M., and Koditschek, D. E., 2001. "Rhex: A simple and highly mobile hexapod robot". *The International Journal of Robotics Research,* ***20***, pp. 616–631.

Appendix: Kinematics Details

This appendix provides a tiny review of the some of the notation and tools developed in [23]. It is intended to provide readers with the bare minimum of mathematical machinery required to replicate the methods presented in Sections 3 and 4.

The hat operator maps twist coordinates to elements of their Lie algebra. In the case of $so(3)$, three parameters are necessary, and thus $\widehat{(...)} : \mathbb{R}^3 \mapsto so(3)$. In the case of $se(3)$, six parameters are needed, and thus $\widehat{(...)} : \mathbb{R}^6 \mapsto se(3)$.

As an example of the $so(3)$ case, suppose $p = (p_1, p_2, p_3)^T$, then

$$\widehat{p} = \begin{bmatrix} 0 & -p_3 & p_2 \\ p_3 & 0 & -p_1 \\ -p_2 & p_1 & 0 \end{bmatrix}. \tag{15}$$

In the case of $se(3)$, suppose $\xi = (v_1, v_2, v_3, \omega_1, \omega_2, \omega_3)^T$, then

$$\widehat{\xi} = \begin{bmatrix} 0 & -\omega_3 & \omega_2 & v_1 \\ \omega_3 & 0 & -\omega_1 & v_2 \\ -\omega_2 & \omega_1 & 0 & v_3 \\ 0 & 0 & 0 & 0 \end{bmatrix}. \tag{16}$$

The wedge operator performs the inverse of the hat, i.e. $(...)^\vee : so(3) \mapsto \mathbb{R}^3$ and $(...)^\vee : se(3) \mapsto \mathbb{R}^6$.

A rigid body transformation is represented with a 4×4 matrix with a special structure

$$g = \begin{bmatrix} R & p \\ 0_{1\times 3} & 1 \end{bmatrix} \in SE(3), \tag{17}$$

where R is a 3×3 rotation matrix and p is a 3×1 translation vector. The matrix exponential maps elements of $se(3)$ to elements of $SE(3)$, i.e. $g = \exp(\widehat{\xi})$ for some $g \in SE(3)$ and $\widehat{\xi} \in se(3)$.

A rigid body transform g is associated with an *adjoint transformation matrix* Ad_g, which maps twist coordinates from one frame into another. The 6×6 adjoint transformation matrix is constructed by

$$Ad_g = \begin{bmatrix} R & \widehat{p}R \\ 0_{3\times 3} & R \end{bmatrix}. \tag{18}$$

For a manipulator with n joints, the *spatial manipulator Jacobian* $J(\theta)$ can be constructed by "stacking" n 6×1 twists, each corresponding to the instantaneous configuration of a manipulator joint

$$J(\theta) = \begin{bmatrix} \xi_1 & \xi_2'(\theta) & ... & \xi_n'(\theta) \end{bmatrix}. \tag{19}$$

The transformed joint twists are given by

$$\xi_i'(\theta) = Ad_g \xi_i, \tag{20}$$

where the ξ_i are defined in Eq 8 and the associated g for each ξ_i is given by

$$g = \exp(\widehat{\xi}_1 \theta_1) ... \exp(\widehat{\xi}_{i-1} \theta_{i-1}). \tag{21}$$